The effect of microscopic friction and size distributions on conditional probability distributions in soft particle packings

Kuniyasu Saitoh · Vanessa Magnanimo · Stefan Luding

Abstract Employing two-dimensional molecular dynamics (MD) simulations of soft particles, we study their non-affine responses to quasi-static isotropic compressions, where the effects of microscopic frictions between the particles in contacts and particle size distributions are examined. To quantify the complicated restructuring of force-chain networks under the isotropic compressions, we introduce the conditional probability distributions (CPDs) of particle overlaps such that a master equation for force distributions in the soft particle packings can be constructed. From our MD simulations, we observe that the CPDs are well described by the q-Gaussian distributions, where we find that the correlation between particle overlaps is suppressed by microscopic frictions, while it significantly increases with the increase of poly-dispersity.

1 Introduction

Mechanical properties of soft particles, e.g. glasses, colloids, and granular materials, have been widely investigated because of their importance in industry

K. Saitoh
WPI Advanced Institute for Materials Research, Tohoku University, 2-1-1 Katahira, Aoba-ku, Sendai 980-8577, Japan
Tel.: +81-22-2176333
E-mail: kuniyasu.saitoh.c6@tohoku.ac.jp

V. Magnanimo
Faculty of Engineering Technology, MESA+, University of Twente, Drienerlolaan 5, 7522 NB, Enschede, The Netherlands

S. Luding
Faculty of Engineering Technology, MESA+, University of Twente, Drienerlolaan 5, 7522 NB, Enschede, The Netherlands

and science. However, their macroscopic responses to quasi-static deformations are still not fully understood due to disordered configurations and complex dynamics of the constituent particles [1]. At microscopic scale, the mechanical response is probed as the change of force-chain networks [2], where non-affine displacements of the constituents cause the complicated restructuring of force-chain networks. Once macroscopic quantities, e.g. stress tensor, are defined as statistical averages over the force-chains, their evolution during quasi-static deformations is described by the change of probability distribution function (PDF) of forces, where many theoretical studies [3,4] have been devoted to determine their functional forms observed in experiments [5] and numerical simulations [6].

Recently, we have proposed a master equation for the PDFs of forces in two-dimensional bi-dispersed frictionless particles [7], which is, in our knowledge, the first attempt to establish a stochastic method for describing the restructuring of force-chains. The master equation can predict the mechanical responses to isotropic compressions and decompressions, where transition rates, or *conditional probability distributions* (CPDs), in the master equation encompass the statistics of microscopic changes of force-chain networks. In addition, any changes of macroscopic quantities defined as the moments of forces (i.e. the coordination number, pressure, and bulk modulus) can be given by the master equation.

In this paper, we generalize our stochastic approach towards wider size distributions and frictional contact models, where the CPDs obtained from MD simulations are compared with our previous study of bi-dispersed frictionless particles [7]. Next, we explain our MD simulations in Sec. 2 and show our numerical results in Sec. 3. Then, we conclude our results in Sec. 4.

2 Method

We use MD simulations of two-dimensional soft particles, where both bi-dispersed and poly-dispersed particles are studied. The number of bi-dispersed particles is $N = 8192$, where we prepare $50 : 50$ binary mixtures of large and small particles with different radii, R_L and R_S, respectively ($R_L/R_S = 1.4$) [7]. On the other hand, the number of poly-dispersed particles is $N = 1872$, where the number of each constituent, N_s, and size ratios are summarized in Table 1 [1]. In our MD simulations, the particle mass, m, is identical and is used for the unit of mass. In addition, for both bi-dispersed and poly-dispersed particles, the normal force between the particles in contact is modeled by a linear spring and dashpot, i.e. $f_{\mathrm{n}ij} = k_\mathrm{n} x_{ij} - \eta_\mathrm{n} \dot{x}_{ij}$, where k_n and η_n are a normal stiffness and normal viscosity coefficient, respectively. Here, the overlap between the particles, i and j, is defined as

$$x_{ij} = R_i + R_j - d_{ij} \tag{1}$$

---

[1] The number of particles and size ratios of poly-dispersed particles are resembling the recent experiments of wooden cylinders [8].

with the interparticle distance, d_{ij}, and particles' radii, R_i and R_j. Thus, the relative speed in the normal direction is given by its time derivative, $\dot{x}_{ij}$. The tangential force is also introduced as $f_{\mathrm{t}ij} = k_{\mathrm{t}}y_{ij} - \eta_{\mathrm{t}}\dot{y}_{ij}$, which is switched to the sliding friction or *Coulomb's friction*, $f_{\mathrm{s}ij} = -\mu|f_{\mathrm{n}ij}|$, if it exceeds the threshold, i.e. if $|f_{\mathrm{t}ij}| > \mu|f_{\mathrm{n}ij}|$. Here, we introduced $k_{\mathrm{t}} = k_{\mathrm{n}}/2$, $\eta_{\mathrm{t}} = \eta_{\mathrm{n}}/4$, and μ as a tangential stiffness, tangential viscosity coefficient, and friction coefficient, respectively. In addition, y_{ij} and $\dot{y}_{ij}$ represent a relative displacement and relative speed in the tangential direction, respectively [9].

To make static packings of the particles, we randomly distribute them in a $L \times L$ square periodic box, where no particle touches others and the friction coefficient is set to zero, $\mu = 0$ (the particles are frictionless during the preparation of static packings). Then, we rescale every radius as $R_i(t + \delta t) = [1 + \{\bar{x} - x_{\mathrm{m}}(t)\}/\lambda] R_i(t)$ $(i = 1, \ldots, N)$, where t, δt, $\bar{x}$, and $x_{\mathrm{m}}(t)$ are time, increment of time, target value of averaged overlap, and averaged overlap at time t, respectively. Here, we use a long length scale $\lambda = 10^2 \bar{\sigma}$ with the mean particle diameter in the final state, $\bar{\sigma}$, to rescale each radius gently [2]. During the rescaling, each radius increases if the averaged overlap is smaller than the target value, $x_{\mathrm{m}}(t) < \bar{x}$, and vice versa, so that the averaged overlap will finally converge to $\bar{x}$. Note that neither particle masses nor the size ratios change during the rescaling, i.e. $\sigma_i(t + \delta t)/\sigma_j(t + \delta t) = \sigma_i(t)/\sigma_j(t)$. We stop the rescaling when every acceleration of particles drops below a threshold, $10^{-6}k_{\mathrm{n}}\bar{\sigma}/m$, and assume that the system is static.

Figure 1(a) displays a static packing of poly-dispersed particles, where the averaged overlap is given by $\bar{x} = 3 \times 10^{-6}\bar{\sigma}$ and each color represents each constituent as listed in Table 1. Figure 1(b) shows the *weighted Delaunay triangulation* (DT) of the static packing, where the red solid lines represent force-chain networks, while the blue solid lines connect the nearest neighbors without contacts. In this figure, we used the *radical-plane construction* [11] to correctly define the nearest neighbors of poly-dispersed particles. In our MD simulations, the distance from jamming is given by the critical scaling of the averaged overlap, $\bar{x} = A(\phi - \phi_J)$ [10], where ϕ and $\phi_J \simeq 0.8458$ are the area fraction of soft particles and the jamming area fraction, respectively. Here, the critical amplitude is found to be $A \simeq 0.25\bar{\sigma}$ (Fig. 2(a)) and the other critical scaling, e.g. the static pressure divided by the normal stiffness (Fig. 2(b)) and the first peak value of the radial distribution function of scaled distances (Fig. 2(c)), are also confirmed, where their power law dependence on the distance from jamming is given by $p/k_{\mathrm{n}} = 1.25 \times (\phi - \phi_J)^{1.04}$ and $g_1 = 0.31 \times (\phi - \phi_J)^{-1}$, respectively [3] [10].

In this study, we investigate mechanical responses of *bi-dispersed frictional particles*, *poly-dispersed frictionless particles*, and *poly-dispersed frictional particles* to isotropic compressions, where the friction coefficients, $\mu = 0$ and

---

[2] We confirmed that static packings prepared with longer length scales, $\lambda = 10^3\bar{\sigma}$ and $10^4\bar{\sigma}$, give the same results concerning their *critical scaling* near jamming [10], while we cannot obtain the same results with a shorter length scale, $\lambda = 10\bar{\sigma}$.

[3] Here, p/k_{n} is dimensionless in two dimensions and the scaled distances for radial distribution functions, $g(r)$, are defined as $r \equiv d_{ij}/(R_i + R_j)$.

Table 1 The number of constituents in poly-dispersed particles, N_s, and each diameter, σ_s ($s = 1, 2, 3, 4$). Each color in Fig. 1(a) is also listed in the last column.

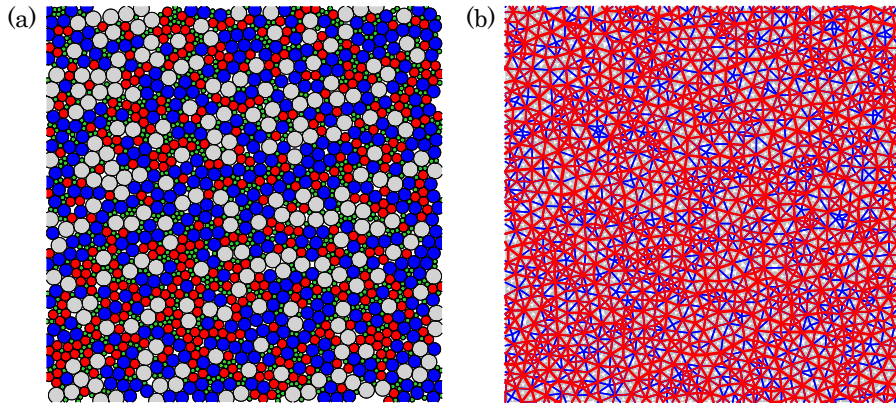| s	N_s	σ_s/σ_4	colors
1	807	0.3	green
2	434	0.6	red
3	414	0.8	blue
4	217	1.0	gray

Fig. 1 (Color online) (a) A static packing of poly-dispersed particles, where the total number of particles is $N = 1872$ and the averaged overlap is given by $\bar{x} = 3 \times 10^{-6}\bar{\sigma}$. (b) The weighted Delaunay triangulation (DT) of the static packing. The red solid lines are equivalent to force-chains, where their widths are proportional to the magnitudes of contact forces. The blue solid lines connect the nearest neighbors without contacts. The gray circles represent the particles.

0.5, are used for frictionless and frictional particles, respectively. To apply an isotropic compression to the system, we rescale every radius as

$$R_i' = \sqrt{1 + \frac{\delta\phi}{\phi}}R_i \ , \qquad (2)$$

where the area fraction increases from ϕ to $\phi + \delta\phi$. After compression, we relax the system until every acceleration of particles drops below the threshold.

3 Results

In this section, we introduce a master equation for the PDFs of particle overlaps as a stochastic description of microscopic changes of force-chain networks. First, we study microscopic responses of overlaps to isotropic compressions (Sec. 3.1), where we describe their mean values and fluctuations in terms of strain increments and distances from jamming (Sec. 3.2). Then, we introduce a
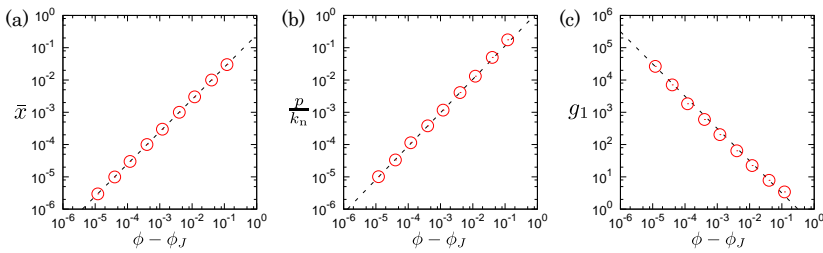
Fig. 2 (Color online) Double logarithmic plots of (a) the averaged overlap, $\bar{x}$, (b) static pressure scaled by the normal stiffness, p/k_n, and (c) first peak value of radial distribution function of scaled distance, g_1, where *poly-dispersed frictionless particles* are used in MD simulations. The dotted lines are power law fittings, (a) $\bar{x} = 0.25\bar{\sigma}(\phi - \phi_J)$, (b) $p/k_\mathrm{n} = 1.25(\phi - \phi_J)^{1.04}$, and (c) $g_1 = 0.31(\phi - \phi_J)^{-1}$, respectively.

master equation for the PDFs of overlaps (Sec. 3.3) and numerically determine transition rates for the master equation (Sec. 3.4).

3.1 Microscopic responses of overlaps

Microscopic responses of soft particle packings to quasi-static deformations are probed as the restructuring of force-chain networks, where particle rearrangements cause the complicated recombination of force-chains, e.g. *opening and closing contacts*. To deal with such the restructuring of force-chain networks, we employ the weighted DT of particle packings as displayed in Fig. 1(b), where not only the particles in contacts, but also the nearest neighbors without contacts, i.e. *virtual contacts*, are connected by the Delaunay edges. We then generalize the definition of particle overlaps from Eq. (1) to

$$x_{ij} \equiv R_i + R_j - D_{ij} \; , \tag{3}$$

where the interparticle distance, d_{ij}, is replaced with the Delaunay edge length, D_{ij}, so that the overlaps between the particles in virtual contacts ($R_i + R_j < D_{ij}$) are defined as negative values. Because the DT is unique for each packing, contacts and virtual contacts are uniquely determined.

If we apply an isotropic compression to the system (Eq. (2)), every generalized overlap, Eq. (3) (not only for contacts, but also for virtual contacts), exhibits *affine responses*,

$$x_{ij}^{\mathrm{affine}} = x_{ij} + \frac{D_{ij}}{2\phi}\delta\phi \; , \tag{4}$$

where we neglected the higher order terms proportional to $x_{ij}\delta\phi$ and $\delta\phi^2$ [7]. However, the particles are randomly arranged such that each force balance is broken by the affine deformation, Eq. (2), where non-affine displacements of the particles restructure the force-chain networks (or the DT) to relax the system to another mechanical equilibrium. After the relaxation, the overlaps
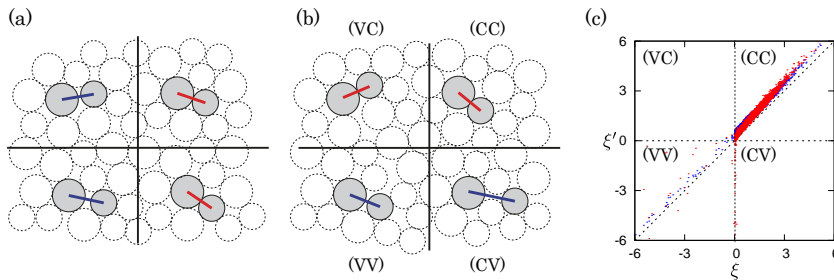
Fig. 3 (Color online) (a) and (b): Sketches of static packings (a) before and (b) after an isotropic compression, where the red and blue solid lines represent contacts and virtual contacts, respectively. The four kinds of transitions, (CC) contact-to-contact, (VV) virtual-to-virtual, (CV) contact-to-virtual, and (VC) virtual-to-contact, are displayed. (c) A scatter plot of scaled overlaps between *poly-dispersed frictional particles*, where the red and blue dots are ξ' and ξ^{affine} plotted against ξ, respectively.

change to new values, $x'_{ij} \neq x^{\mathrm{affine}}_{ij}$, that is *non-affine responses* of generalized overlaps.

As shown in Figs. 3(a) and (b), there are only four kinds of transitions from x_{ij} to x'_{ij}: Positive overlaps, $x_{ij} > 0$, remain as positive, $x'_{ij} > 0$, or negative overlaps, $x_{ij} < 0$, remain as negative, $x'_{ij} < 0$, where they do not change their signs and thus contacts are neither generated nor broken. We call these changes *contact-to-contact* (CC) and *virtual-to-virtual* (VV), respectively. It is also possible that positive overlaps change to negative ones and negative overlaps become positive, where existing contacts are broken and new contacts are generated, respectively. We call these changes opening and closing contacts, or in analogy to the above, *contact-to-virtual* (CV) and *virtual-to-contact* (VC), respectively.

In the following, we scale the generalized overlaps, Eq. (3), by the averaged overlap before compression, $\bar{x}$, such that scaled overlaps before deformation, after affine deformation, and after relaxation are introduced as $\xi \equiv x_{ij}/\bar{x}$, $\xi^{\mathrm{affine}} \equiv x^{\mathrm{affine}}_{ij}/\bar{x}$, and $\xi' \equiv x'_{ij}/\bar{x}$, respectively (we omit the subscript, ij, after the scaling). From the affine responses, Eq. (4), and the critical scaling of the averaged overlap, $\bar{x} = A(\phi - \phi_J)$, the scaled overlap after affine deformation is given by a linear function of ξ,

$$\xi^{\mathrm{affine}} = \xi + B_a \gamma , \tag{5}$$

where the offset, $B_a \gamma \equiv (D_{ij}/2A\phi)\gamma$, is proportional to the scaled strain increment, $\gamma \equiv \delta\phi/(\phi - \phi_J)$. On the other hand, we will find that the scaled overlap after relaxation, ξ', fluctuates around the mean value due to the restructuring of force-chain networks.

3.2 Mean and fluctuations of overlaps

To describe non-affine responses of scaled overlaps, ξ', we measure their mean values and fluctuations through scatter plots of ξ and ξ'. Figure 3(c) displays

the scatter plot for *poly-dispersed frictional particles*, where the four different transitions are mapped onto four regions: (CC) $\xi, \xi' > 0$, (VV) $\xi, \xi' < 0$, (CV) $\xi > 0$, $\xi' < 0$, and (VC) $\xi < 0$, $\xi' > 0$, respectively. In this figure, affine responses of scaled overlaps, ξ^{affine}, are described by the deterministic equation (5), while non-affine responses, ξ', distribute around mean values with finite fluctuations. The differences between affine and non-affine responses are always present, but small if the applied strain is small or the system is far from jamming such that the scaled strain increment is significantly small, $\gamma \ll 1$, while ξ' deviates more from ξ^{affine} and data points are more dispersed if $\gamma \gg 1$.

In a similar way to affine responses, Eq. (5), we describe the mean values of ξ' in CC and VV regions by linear functions of ξ,

$$m_s(\xi) = (a_s + 1)\xi + b_s \ , \tag{6}$$

where the subscripts, $s = c$ and v, represent the mean values in CC and VV, respectively. Introducing standard deviations of ξ' from their mean values as v_s (which are almost independent of ξ), we quantify the systematic deviation from affine responses by the coefficients, a_s, b_s, and v_s, where affine responses, Eq. (5), can be recovered if $a_s = v_s = 0$ and $b_s = B_a\gamma$. Figure 4 displays the coefficients, a_s, b_s, and v_s ($s = c, v$), for *poly-dispersed frictional particles* plotted against the scaled strain increment, γ. In this figure, we find that all the coefficients, except for $a_v \simeq 0$, increase with the scaled strain increment, where the data with a wide variety of $\delta\phi$ and $\phi - \phi_J$ collapse onto the linear scaling,

$$a_c = A_c\gamma \ , \quad b_s = B_s\gamma \ , \quad v_s = V_s\gamma \ , \tag{7}$$

in the fitting range, $10^{-6} \leq \gamma \leq 5 \times 10^{-3}$. Here, the scaling amplitudes are given by $A_c = 0.39$, $B_c = 0.81$, $B_v = 1.32$, $V_c = 0.30$, and $V_v = 1.22$. Note that virtual contacts behave like affine responses in average (because $a_v \simeq 0$ and $B_v \approx B_a \simeq 1.3$ in average), except for their huge fluctuations ($V_v \gg V_c$).

3.3 A master equation for the PDFs of overlaps

The restructuring of force-chain networks attributed to the transitions (CC, VV, CV, and VC) is well captured by the PDFs of scaled overlaps. In the following, we introduce the PDF as $P_\phi(\xi)$ with the subscript, ϕ, representing the area fraction of soft particles. Because the total number of Delaunay edges is conserved during deformations, the PDFs are normalized as

$$\int_{-\infty}^{\infty} P_\phi(\xi)d\xi = 1 \ . \tag{8}$$

In our previous study of bi-dispersed frictionless particles [7], we found that the affine responses, Eq. (5), just shifted the PDF to the positive direction, while the non-affine responses broadened the PDF in positive overlaps and
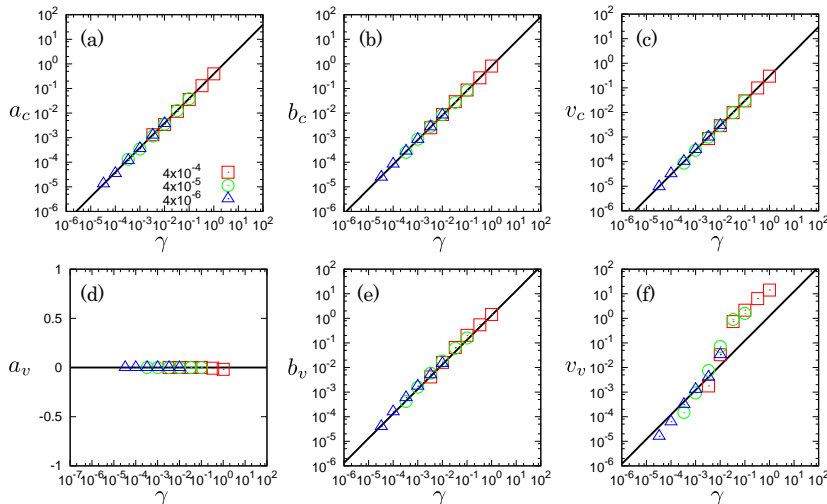
Fig. 4 (Color online) Double logarithmic plots of the coefficients for mean values and fluctuations of scaled overlaps, (a) a_c, (b) b_c, (c) v_c, (e) b_v, and (f) v_v, and a semi-logarithmic plot of (d) a_v, as functions of the scaled strain increment, γ. Here, we applied different strain increments, $\delta\phi = 4 \times 10^{-4}$, 4×10^{-5}, and 4×10^{-6} (as indicated by the symbols in the legend of (a)), to *poly-dispersed frictional particles* with different distances from jamming, $\phi - \phi_J = 1.2 \times 10^{-1}$, 4×10^{-2}, 1.2×10^{-2}, 4×10^{-3}, 1.2×10^{-3}, and 4×10^{-4}. The solid lines represent the linear scaling, Eq. (7), where the fitting range is given by $10^{-6} \leq \gamma \leq 5 \times 10^{-3}$.

generated a discontinuous "gap" around zero [4]. We also find that the PDF of negative overlaps after non-affine deformation is comparable with that after affine deformation. In our simulations of poly-dispersed frictional particles, we observe similar results. Figure 5 displays the PDFs for poly-dispersed frictional particles, where the PDF before compression, $P_\phi(\xi)$, has a discontinuous gap around zero. The affine deformation pushes the PDF towards the positive direction as $P_{\phi+\delta\phi}(\xi^{\text{affine}})$, where the poly-dispersity smooths out the discontinuity around zero. After non-affine deformation, the PDF widens in positive overlaps as $P_{\phi+\delta\phi}(\xi')$, while there is no significant difference between $P_{\phi+\delta\phi}(\xi^{\text{affine}})$ and $P_{\phi+\delta\phi}(\xi')$ in negative overlaps (the inset in Fig. 5).

To describe such the non-affine evolution of the PDFs, we connect the PDF after non-affine deformation to that before compression through the Chapman-Kolmogorov equation [13],

$$P_{\phi+\delta\phi}(\xi') = \int_{-\infty}^{\infty} W(\xi'|\xi)P_\phi(\xi)d\xi , \qquad (9)$$

assuming that transitions between overlaps (from ξ to ξ') can be considered as *Markov processes*. On the right-hand-side of Eq. (9), the CPD of scaled overlaps, ξ', which were ξ before compression, is introduced as $W(\xi'|\xi)$. By

---

[4] Such a discontinuity is specific to static packings, where a corresponding gap has been observed in a radial distribution function in the glass with zero-temperature [12].
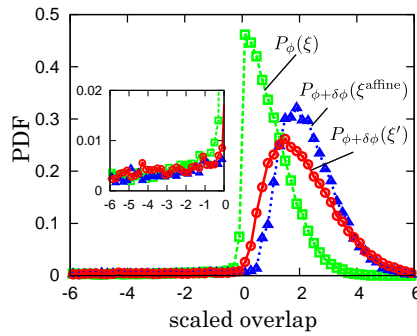
Fig. 5 (Color online) The PDFs of scaled overlaps in *poly-dispersed frictional particles* before compression, $P_\phi(\xi)$ (the squares), after affine deformation, $P_{\phi+\delta\phi}(\xi^{\text{affine}})$ (the triangles), and after non-affine deformation, $P_{\phi+\delta\phi}(\xi')$ (the circles), where the inset is a magnification of the PDFs of negative scaled overlaps.

definition, the CPD is normalized as $\int_{-\infty}^{\infty} W(\xi'|\xi)d\xi' = 1$. Then, a master equation for the PDFs is derived from the Chapman-Kolmogorov equation (9) as [13]

$$\frac{\partial}{\partial\phi}P_\phi(\xi') = \int_{-\infty}^{\infty} \left\{ T(\xi'|\xi)P_\phi(\xi) - T(\xi|\xi')P_\phi(\xi') \right\} d\xi \qquad (10)$$

with the transition rate defined as $T(\xi'|\xi) = \lim_{\delta\phi\to 0} W(\xi'|\xi)/\delta\phi$. The first and second terms on the right-hand-side of the master equation (10) represent the gain and loss of new overlaps, ξ', respectively. Therefore, the transition rates or the CPDs fully determine the statistics of microscopic responses of force-chain networks.

3.4 Conditional probability distributions of overlaps

To understand the restructuring of force-chain networks, we numerically determine the CPDs of scaled overlaps, where the CPDs are given by the distributions of ξ' around the mean values, $m_s(\xi)$. Note that the CPD for affine responses is given by a delta function, $W_{\text{affine}}(\xi'|\xi) = \delta(\xi' - \xi^{\text{affine}})$, which just shifts the PDF by $B_a\gamma$ [5]. However, non-affine deformations generate fluctuations of scaled overlaps around their mean values so that the CPDs are given by distributions with finite widths. In our previous study of bi-dispersed frictionless particles [7], we have confirmed that the CPDs for CC and VV transitions are well described by $\gamma W_{CC}(\xi'|\xi) = f_c(\Xi_c/\gamma)$ and $\gamma W_{VV}(\xi'|\xi) = f_v(\Xi_v/\gamma)$, respectively, where $\Xi_s \equiv \xi' - m_s(\xi)$ $(s = c, v)$ is the distance from the mean values and

$$f_s(x) = \frac{1}{c(q_s)} \left[1 + \frac{x^2}{n(q_s)V_s^2} \right]^{\frac{1}{1-q_s}} \qquad (11)$$

---

[5] From the Chapman-Kolmogorov equation (9), $P_{\phi+\delta\phi}(\xi') = \int_{-\infty}^{\infty} \delta(\xi' - \xi^{\text{affine}})P_\phi(\xi)d\xi = \int_{-\infty}^{\infty} \delta(\xi' - B_a\gamma - \xi)P_\phi(\xi)d\xi = P_\phi(\xi' - B_a\gamma)$.

is the *q-Gaussian distribution* [14] with the functions defined as $n(t) = (t - 3)/(1 - t)$ and $c(t) = V_s\sqrt{n(t)}B(1/2, n(t)/2)$ [6]. The shape of the CPD is characterized by the *q-index*, q_s, which is in the range between $1 < q_s < 3$, where the normal (Gaussian) distribution corresponds to the limit, $q \to 1$.

In the following, we compare our previous results of the CPDs for bi-dispersed frictionless particles [7] with those for *bi-dispersed frictional particles*, *poly-dispersed frictionless particles*, and *poly-dispersed frictional particles* to examine the effects of microscopic frictions and particle size-distributions on the restructuring of force-chain networks.

3.4.1 Bi-dispersed frictional particles

First, we examine the dependence of the CPDs on microscopic frictions between the particles in contacts. Figure 6 displays the CPDs obtained from our MD simulations of *bi-dispersed frictional particles*, where the different symbols represent different values of the scaled strain increment, γ. Note that Figs. 6(b) and (d) are semi-logarithmic plots of Figs. 6(a) and (c), respectively. In this figure, all the data are well collapsed if we multiply the CPDs and distances from the mean values by γ and $1/\gamma$, respectively, which means that the CPDs for CC and VV transitions are *self-similar* against the change of scaled strain increment, γ. The solid lines are the *q*-Gaussian fits to the CPDs, where the *q*-indices for CC and VV transitions are given by $q_c^{\mathrm{BN}} = 1.06$ (Figs. 6(a) and (b)) and $q_v^{\mathrm{BN}} = 1.21$ (Figs. 6(c) and (d)), respectively. We then find that the CPDs for CC transitions are nicely *symmetric* around the mean values, $m_c(\xi)$, while those for VV transitions deviate from the symmetric *q*-Gaussian distributions, which might be caused by the microscopic frictions. We also plot the *q*-Gaussian fits to our previous results of bi-dispersed frictionless particles (the dotted lines) [7], where the *q*-indices for CC and VV transitions are given by $q_c^{\mathrm{BL}} = 1.13 > q_c^{\mathrm{BN}}$ and $q_v^{\mathrm{BL}} = 1.39 > q_v^{\mathrm{BN}}$, respectively. Therefore, the tails of the CPDs for bi-dispersed frictional particles are narrower than those for bi-dispersed frictionless particles, implying that the correlations of scaled overlaps are suppressed by the microscopic frictions.

3.4.2 Poly-dispersed frictionless particles

Next, we study the effect of size-distributions on the CPDs. Figure 7 shows the CPDs for *poly-dispersed frictionless particles*, where the different symbols represent different values of γ. In this figure, all the data are collapsed after the same scaling as in Fig. 6. In addition, both the CPDs for CC and VV transitions are symmetric around the mean values and are well described by the *q*-Gaussian distributions (the solid lines), where their *q*-indices are given by $q_c^{\mathrm{PL}} = 1.37 > q_c^{\mathrm{BL}}$ (Figs. 7(a) and (b)) and $q_v^{\mathrm{PL}} = 1.79 > q_v^{\mathrm{BL}}$ (Figs. 7(c) and (d)), respectively. Therefore, the basic properties of the CPDs found in our previous study [7], i.e. their self-similarity and symmetry, are not affected by
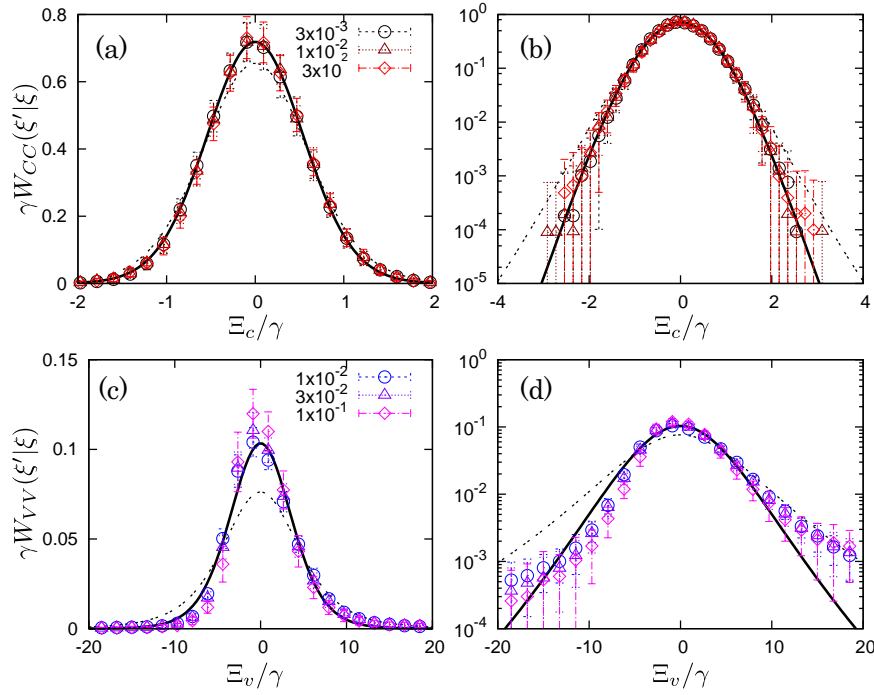
---

[6] $B(x, y)$ is the beta function.

Fig. 6 (Color online) The CPDs for (a) CC and (c) VV transitions multiplied by the scaled strain increment, γ, and plotted against scaled distances from the mean values, Ξ_s/γ ($s = c, v$), where (b) and (d) are semi-logarithmic plots of (a) and (c), respectively. The *bi-dispersed frictional particles* are used in the MD simulations, where the different symbols represent different values of γ as listed in the legends of (a) and (c). The solid lines are the q-Gaussian distributions with the q-indices, $q_c^{\mathrm{BN}} = 1.06$ and $q_v^{\mathrm{BN}} = 1.21$, respectively. The dotted lines are the q-Gaussian distributions obtained from our previous study of bi-dispersed frictionless particles [7], where the q-indices for CC and VV transitions are given by $q_c^{\mathrm{BL}} = 1.13 > q_c^{\mathrm{BN}}$ and $q_v^{\mathrm{BL}} = 1.39 > q_v^{\mathrm{BN}}$, respectively.

size-distributions, while the CPDs for poly-dispersed frictionless particles have wider tails than those for bi-dispersed frictionless particles (the dotted lines in Fig. 7) [7], implying that the correlations of scaled overlaps significantly increase with the increase of poly-dispersity [15].

3.4.3 Poly-dispersed frictional particles

We have observed that microscopic frictions between the particles in contacts narrow the tails of the CPDs, while the tails widen with the increase of poly-dispersity. Thus, the correlation of scaled overlaps is either suppressed by the microscopic frictions or enhanced by the poly-dispersity of soft particles. Here, we test both effects on the CPDs to clarify which one is significant for the restructuring of force-chains. Figure 8 displays the CPDs for *poly-dispersed frictional particles*, where the different symbols represent different values of the scaled strain increment, γ. In this figure, all the data are collapsed after the
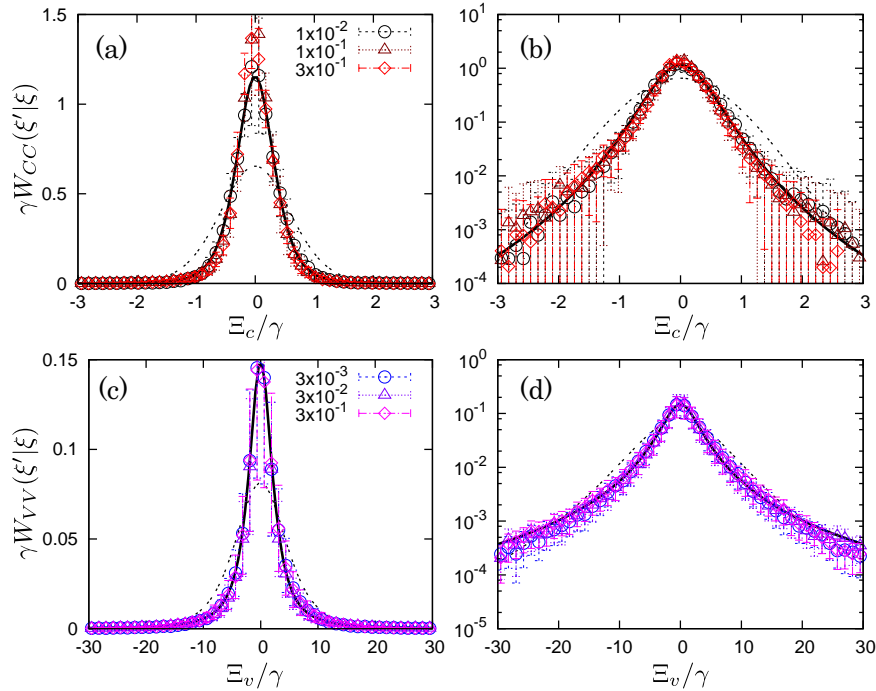
Fig. 7 (Color online) The CPDs for (a) CC and (c) VV transitions after the same scaling as in Fig. 6, where (b) and (d) are semi-logarithmic plots of (a) and (c), respectively. The *poly-dispersed frictionless particles* are used in the MD simulations, where the different symbols represent different values of the scaled strain increment, γ, as listed in the legends of (a) and (c). The solid lines are the q-Gaussian distributions with the q-indices, $q_c^{\mathrm{PL}} = 1.37 > q_c^{\mathrm{BL}}$ and $q_v^{\mathrm{PL}} = 1.79 > q_v^{\mathrm{BL}}$, respectively, while the dotted lines are as in Fig. 6.

same scaling (as in Fig. 6) and the CPDs for CC transitions are well fitted by the q-Gaussian distribution, where the q-index is given by $q_c^{\mathrm{PN}} = 1.19 \simeq q_c^{\mathrm{BL}}$ (the solid lines in Figs. 8(a) and (b)) such that the effect of microscopic frictions and that of poly-dispersity compete with each other. However, the CPDs for VV transitions slightly deviate from the symmetric q-Gaussian distribution (the solid lines in Figs. 8(c) and (d)) such that the microscopic frictions violate the symmetry of the CPDs, where the best fit to our numerical results gives the q-index, $q_v^{\mathrm{PN}} = 1.09 < q_v^{\mathrm{BL}}$. Therefore, microscopic frictions are more significant than the poly-dispersity for correlations between virtual contacts.

4 Summary

In this study, we have investigated mechanical responses of *bi-dispersed frictional particles*, *poly-dispersed frictionless particles*, and *poly-dispersed frictional particles* to isotropic compressions by two-dimensional MD simulations. The complicated restructuring of force-chain networks during relaxation has
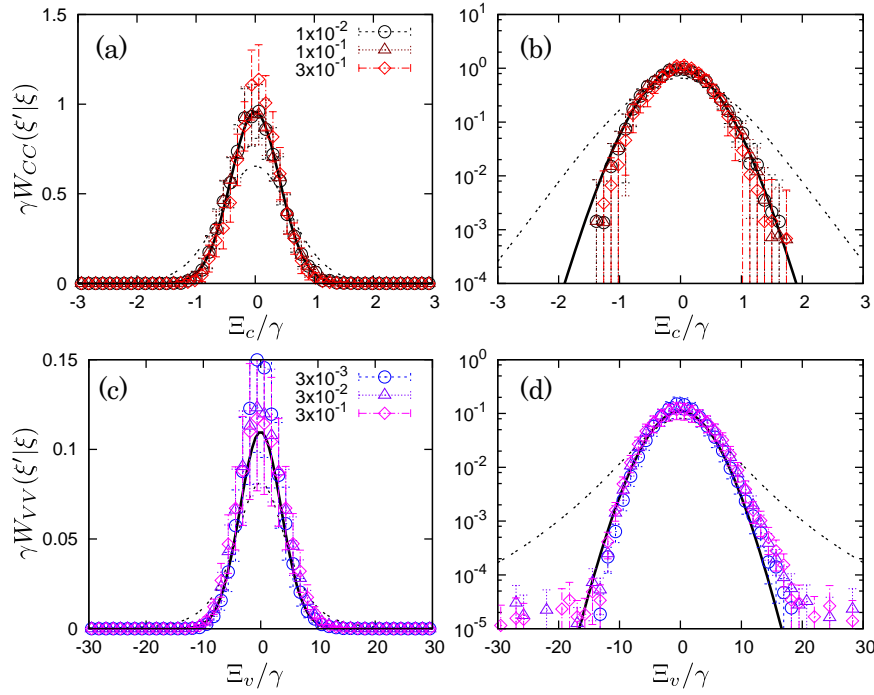
Fig. 8 (Color online) The CPDs for (a) CC and (c) VV transitions after the same scaling as in Fig. 6, where (b) and (d) are semi-logarithmic plots of (a) and (c), respectively. The *poly-dispersed frictional particles* are used in the MD simulations, where the different symbols represent different values of the scaled strain increment, γ, as listed in the legends of (a) and (c). The solid lines are the q-Gaussian distributions with the q-indices, $q_c^{\mathrm{PN}} = 1.19 \simeq q_c^{\mathrm{BL}}$ and $q_v^{\mathrm{PN}} = 1.09 < q_v^{\mathrm{BL}}$, respectively, while the dotted lines are as in Fig. 6.

Table 2 The q-indices for the CPDs in CC and VV, where q_s^{BL}, q_s^{BN}, q_s^{PL}, and q_s^{PN} are those for bi-dispersed frictionless particles [7], bi-dispersed frictional particles, poly-dispersed frictionless particles, and poly-dispersed frictional particles, respectively.

s	q_s^{BL}	q_s^{BN}	q_s^{PL}	q_s^{PN}
c	1.13	1.06	1.37	1.19
v	1.39	1.21	1.79	1.09

been described by the stochastic approach to non-affine deformations, i.e. the mean and fluctuations of generalized overlaps, where the deviation from affine deformations is quantified by the slope (a_s) and offset (b_s) for the mean values, and standard deviation (v_s) of the fluctuations. As we found in our previous study of bi-dispersed frictionless particles [7], those coefficients (a_s, b_s, and v_s) for poly-dispersed frictional particles are also proportional to the scaled strain increment, $\gamma = \delta\phi/(\phi - \phi_J)$. We have found that the deviation from affine responses significantly increases with the increase of γ, while the responses of virtual contacts are mostly affine in average (except for their huge

fluctuations). After the non-affine deformations of poly-dispersed frictional particles, the PDFs of generalized overlaps are broadened in the positive side (i.e. real contacts), while their changes in the negative side (i.e. virtual contacts) are almost the same with affine deformations. We have introduced the Chapman-Kolmogorov equation (9) and master equation (10) to describe the non-affine evolution of the PDFs, where the statistics of microscopic responses of generalized overlaps are fully determined by the CPDs, $W(\xi'|\xi)$, and transition rates, $T(\xi'|\xi)$. To understand the effects of microscopic frictions and size-distributions on the restructuring of force-chain networks, we have compared our results of the CPDs with the previous study of bi-dispersed frictionless particles [7], where the shapes or tails of the CPDs are well characterized by the q-indices in the q-Gaussian distributions (Table 2). We have found that the tails of the CPDs for bi-dispersed frictional particles are narrower than those for bi-dispersed frictionless particles such that correlations of contacts and virtual contacts are suppressed by the microscopic frictions (Fig. 6). On the other hand, the tails of the CPDs for poly-dispersed frictionless particles are much wider than those for bi-dispersed frictionless particles so that the correlations are significantly increased by the increase of poly-dispersity (Fig. 7). The same trends have been observed in MD simulations of poly-dispersed frictional particles (Fig. 8). It should be noted that the self-similarity of the CPDs has been confirmed, regardless microscopic frictions and size-distributions, where all the CPDs are nicely collapsed after the scaling by γ. However, the symmetry of the CPDs for VV transitions might be violated by microscopic frictions (Figs. 6(d) and 8(d)), where we need more systematic studies of the dependence of the CPDs on the microscopic friction coefficient, μ.

In conclusion, the restructuring of force-chain networks during non-affine deformations is described by the stochastic approach to generalized overlaps. The non-affinity of their microscopic changes increases with the scaled strain increment, though their statistics are governed by the self-similar conditional probabilities. From the shapes of the CPDs, it was found that correlations of generalized overlaps are suppressed (increased) by microscopic frictions (poly-dispersity).

References

1. J. Lemaitre, J.L. Chaboche, *Mechanics of Solid Materials* (Cambridge University Press, Cambridge, UK, 1990)

2. T.S. Majmudar, M. Sperl, S. Luding, R.P. Behringer, Phys. Rev. Lett. **98**, 058001 (2007)
3. S. Henkes, B. Chakraborty, Phys. Rev. E **79**, 061301 (2009)
4. J.H. Snoeijer, T.J.H. Vlugt, M. van Hecke, W. van Saarloos, Phys. Rev. Lett. **92**, 054302 (2004)
5. D.M. Mueth, H.M. Jaeger, S.R. Nagel, Phys. Rev. E **57**, 3164 (1998)
6. L.E. Silbert, G.S. Grest, J.W. Landry, Phys. Rev. E **66**, 061303 (2002)
7. K. Saitoh, V. Magnanimo, S. Luding, Soft Matter **11**, 1253 (2015)
8. G. Combe, V. Richefeu, M. Stasiak, A.P. Atman, Phys. Rev. Lett. **115**, 238301 (2015)
9. S. Luding, J. Phys.: Condens. Matter **17**, S2623 (2005)
10. M. van Hecke, J. Phys.: Condens. Matter **22**, 033101 (2010)
11. S. Sastry, D.S. Corti, P.G. Debenedetti, F.H. Stillinger, Phys. Rev. E **56**, 5524 (1997)
12. H. Jacquin, L. Berthier, F. Zamponi, Phys. Rev. Lett. **106**, 135702 (2011)
13. N.G. van Kampen, *Stochastic Processes in Physics and Chemistry, 3rd edition* (Elsevier B. V. Amsterdam, The Netherlands, 2007)
14. C. Tsallis, J. Stat. Phys. **52**, 479 (1988)
15. V. Ogarko, S. Luding, Soft Matter **9**, 9530 (2013)